Received: 15 March 2022 | Revised: 13 June 2022 | Accepted: 29 June 2022

IET Wireless Sensor Systems

DOI: 10.1049/wss2.12040

The Institution of Engineering and Technology WILEY

ORIGINAL RESEARCH

Use of wireless sensor network system based on water level, rain, conductivity, oil and turbidity sensors to monitor the storm sewerage

Javier Rocher[1] | Albert Rego[2] | Jaime Lloret[1] | Luís M. L. Oliveira[3]

[1]Instituto de Investigación para la Gestión Integrada de Zonas Costeras, Universitat Politècnica de València, Valencia, Spain

[2]Universidad Europea de Valencia, Valencia, Spain

[3]Department of Informatics, Instituto Politécnico de Tomar, Tomar, Portugal

Correspondence

Javier Rocher, Instituto de Investigación para la Gestión Integrada de Zonas Costeras, Universitat Politècnica de València, Camino de Vera, s/n, 46022 Valencia, Spain.
Email: jarocmo@doctor.upv.es

Funding information

Ministerio de Educación, Cultura y Deporte, Grant/Award Number: FPU16/05540

Abstract

Storm sewerages are crucial infrastructures in water management. In this paper, a system was developed to detect the blockage of the sewerage and the presence of illegal spills in Storm sewerages. Different nodes with sensors measuring the water level, turbidity, conductivity, and oil presence are scattered in the sewerage. These nodes are connected to a master node for processing the information with a rain sensor. The rain and water level sensors are used to determine one of the four possibilities regarding the presence of water in the sewerage and whether it is raining. According to the combinations, it can be determined whether it is a normal situation or there are spills or blockages. It is shown that there are differences between sewerage with and without blockage via the water level. This can be used to determine the presence of a blockage. The identification of an illegal spill is performed with the use of conductivity, turbidity, and oil sensors. The authors determined that yellow and infrared light can determine the oil concentration in the oil sensor in a range of 0–2.2 mL oil/L water with yellow light and 0.4–20 mL oil/L water with infrared light. Finally, the conductivity sensor can determine water conductivity from 0.526 to 58.4 mS/cm.

1 | INTRODUCTION

Water is an essential resource for life that is included within the 2030 agenda of the United Nations in Goal 6 with the caption "Ensure access to water and sanitation for all" [1]. There are different sanitation structures like WasteWater Treatment Plants (WWTP), sewerage, and storm tanks to ensure water sanitation. Sewerage is a set of pipelines used to transport the wastewater and runoff out of the cities. We can differentiate 3 types of sewerage, (I) combined sewerage, (II) sanitary sewerage, and (III) storm sewerage [2]. The sanitary sewers transport the wastewater from urban areas to the WWTP. Storm sewers are used to transport the urban runoff to a water body. Finally, the combined sewerage mixes the wastewaters with runoff and transports the water to WWTP. Storm tanks prevent inundation in the cities or an excess of water in the WWTPs by storing excess rain.

The water of the storm sewerage systems can present problems of pollution. Xu et al. [3] showed three main reasons by which sewerage can pollute rivers. (I) Incomplete sewer system, (II) Damaged sewer pipelines, and (III) Illicit connection to stormwater sewerage. According to the illicit connections, every substance can be dumped in the storm sewerage. The illicit connection can cause spills of untreated wastewater, which can cause problems in the different nearby areas of the spill point [4]. Storm sewerage can be affected by different pollutants. In the storm sewerage of Paris, they found metals, PAHs, PCBs, organotin compounds, alkylphenols, phthalates, pesticides, and VOCs as pollutants [5]. Other cases are in Missouri and Monterey (United States of America). The governments listed the main pollutants in the storm sewage (antifreeze, fertilisers, motor oil, paint, pesticides, etc. [6, 7]). The sources of these pollutants are the illicit discharges from industrial or commercial activities in the storm sewerage and the dragging of these pollutants by the rainwater. The discharges from industrial parks or commercial activities that are dumped in the sewerage are inspected regularly. However, they are not monitored continuously; thus, accidental or not, spills

can occur [8]. In the Valencia region, in 2020, 3299 high loads of industrial discharges were detected. Of all the discharges produced, only the responsible person has been detected in 290 cases (8.8%) [9]. In 2019, Toronto water management detected 654 non-compliances under the Sewers law in 2860 inspections [10].

Different solutions such as spatial information [11], level sensors, and water quality monitoring inversed optimisation models [12] are proposed to reduce the stormwater pollution problems in the storm sewerage. In addition, the use of sensor networks allows optimising operational efficiency, automation, maintenance, and rationalisation. Moreover, the use of networks permits the interconnection between machines and people [13]. Thus, the Wireless Sensor Network (WSN) is a good tool to reduce the number of illicit spills since it allows detection and, therefore, acts more quickly on those responsible.

One problem with the use of WSN is the maintenance that the nodes need. Using sensors based on chemical reactions (analysers) or membranes increases the maintenance costs because the membranes tend to clog and degrade. The use of chemical sensors is essential to refill the chemical bottles. This is a motivation to use sensors based on physical parameters. However, these can also be faulty. To identify faults in sensors, different statistical techniques have been developed, such as (I) comparing the value with nearest-neighbour, (II) Artificial neural networks, (III) Use of clusters, and (IV) classification techniques [14, 15]. A statistical technique used in sewage is sensor failure detection and faulty data accommodation (SFDFDA) [16]. This technique uses the data collected previously to predict the value of a variable. With this prediction, the value is compared to the sensor's measurement. If the system detects significant differences, the abnormal data is isolated.

In this paper, we show a WSN to detect the presence of illicit spills and blockages in the storm sewerage. Our proposal uses rain, water level, oil, turbidity, and conductivity sensors to determine the presence of illicit spills in the sewerage and blockages in the storm sewerage networks. We use the rain sensor to control the presence and amount of rain in the monitoring area and the level sensor to monitor the presence of water in the pipes. We establish four different scenarios according to the rain and water level in the sewer. The perfect scenario for an illicit discharge is when it is raining and there is water in the storm pipes. In this scenario, the rain and level sensors cannot monitor the presence of illicit spills. We use turbidity, oil, and conductivity sensors to solve this problem. Turbidity and oil sensors are based on the use of different colours of light captured by a photoreceptor to monitor the value of oil or turbidity in the water. We use a photodiode and a light-dependent resistor (LDR) as photoreceptors. The conductivity sensor used is an inductive sensor based on two coils. If the concentration of turbidity, conductivity, and oil presence values are normal (there is no spill), our system uses the water level to detect the presence of a blockage in the pipe. The other three scenarios are (I) a normal condition if it is not raining and there is no water in the pipe. (II) surface blockage if it is raining and there is no water in the pipes. (III) Spill if it is not raining and there is water in the pipe.

The rest of the paper is structured as follows. Section 2 presents different studies related to monitoring sewerage, conductivity, oil, and turbidity sensors. The design proposal is presented in Section 3. The methodology used in the experiment is presented in Section 4. In Section 5, we present the results of our experiments. Finally, in Section 6, the conclusions are shown.

2 | RELATED WORK

In this section, we analyse different papers about the use of sensors in sewerage. First, we show the use of sensors in sewerage. Then, in section 2.2, we analyse different solutions to monitor water conductivity. Turbidity sensors are analysed in section 2.3. Finally, we study different propositions of oil sensors in section 2.4.

2.1 | Monitoring sewerage

In this subsection, we study different works about the use of sensors to monitor illegal connections and spills.

One method to detect illicit connections is the use of temperature sensors. Nienhuis et al. [17] proposed the use of fibre-optic cables as temperature sensors to detect illicit connections in storm sewerage. They located three sensors in the bottom and top of the sewerage and floating on the water. With the variation of the temperature, they detected illicit connections. Of the three positions tested, the cable in the bottom of the pipe presents challenge in detecting the spills. However, the other two work well. In addition, the distance between the connection and the sensing point has an important effect on the detection. Another system based on optical fibre is presented by Vosse et al. [18]. They determined the noise levels in the measurements of the temperature at the different distances for 2 h. Then, they compared the temperature of the water with the value of the noise. The sensor sends an alarm if there is an important difference between the measured temperature and the noise. The measurements were elaborated twice to improve the performance of the sensor. With this system, the authors have detected 99 of 100 artificial spills. In our opinion, temperature sensors are useful for monitoring illicit connections in the sewerage. However, they have important gaps. (I) Some spills do not change the temperature of the water. (II) The use of only temperature sensors cannot detect them. (III) The impact of solids can damage the fibre optical sensor present in the sewerage.

Other authors have proposed using more parameters to detect abnormal situations in sewerage. Irvine et al. [19] studied the use of different parameters and their cost for controlling the illicit discharge of wastewater into the storm sewer in Western New York State. They determined that temperature parameters, pH, conductivity, *Escherichia coli*, ammonia, nitrate, fluoride, total chlorine, potassium, detergents, phosphorous, and turbidity can be used to determine the presence of illegal spills and the possible source (industry,

irrigation water, wash water, and sanitary water). The main gap in this proposal is the use of many parameters. In great networks of sewerage, controlling these parameters is too expensive. Other authors reduce the number of parameters to detect abnormal values. Li et al. [20] propose monitoring 4 parameters (temperature, pH, conductivity, and turbidity). They used a pump to capture sewerage water to the sensing unit, where it has a data processing and communication unit to transfer the data; its system was tested for 3 years in different sewerages. Due to the presence of solids and the generation of biofilms in the system, the authors studied the use of a diameter channel in the sensing unit of 14 mm, with a current flow between 40 and 60 L/min. They determined that the system sustained for 12 months without blockage and significant biofilm formations. Thanks to the system, different abnormal events have been detected related to illegal industrial discharges to the sewerage. This proposal's main gap is the energy cost of pumping the water. It can be unaffordable to big networks.

2.2 | Conductivity sensor

The conductivity is defined as the capacity of the water to transport an electric current. Conductivity is related to the concentration and the type of salt in the water. In this subsection, we show different techniques to determine the conductivity of the water.

The standard methods to determine the conductivity are conductivity cells and density methods. Conductivity cells are based on different platinised or non-platinised electrodes immersed in water and calibrated with a solution of 0.01 M KCl at the temperature of 25°C. [21]. Usually, the commercial conductimeters have a temperature sensor to adjust the measurement of conductivity to 25°C. The other standard method is the density method. It is based on passing the sample through a vibrating tube. The difference between the density of pure water and the sample is related to the salinity. Now, the use of conductivity cells is more popular than that of density methods. An example of a conductivity cell is proposed by Carminati and Luzzatto-Fegiz [22]. They used a micro-USB cable as the electrode, an Arduino Uno as microcontroller, an AD5933 to convert the signal, and different electronic elements to generate and receive voltage. They determined that the sensor has a resolution of 0.1% and a good adjustment between measuring a commercial conductivity in the range of 3.5–0.5 S/m. Conductivity cells are frequently used to monitor the conductivity of the water. However, it is not the best option to monitor the conductivity of the sewerage. Due to the fact that there may be solids in sewerage that impact the electrodes and change the distance between them, and it will be out of calibration. In addition, since the sensor is in contact with water, its electrodes can oxidise or change their chemical structure over time.

A solution to avoid water contact with the sensor is the use of coupled contactless conductivity detection (C4D). C4D is a new methodology currently being investigated. Huang et al. [23] developed a new C4D sensor based on two electrodes. An AC current powers one electrode, and the other electrode is induced. These electrodes are located on a pipe of 1.8 and 3.2 mm of diameter. The results show that the sensor can work between 0.1348 and 105.3 mS/cm with less than 3.5% relative error. The main gap in the use of C4D is the diameter of the pipe. These proposals are good for small diameter applications but not for big diameters of pipes. Other inductive sensors can be used to monitor water conductivity. Kandur et al. [24] show a transformer-type inductive conductivity sensor as a low-cost sensor to measure the conductivity in different temperatures. They used two coils with a core of Mn-Zn encapsulated in resin. The conductivity samples tested were between 0 and 55 mS/cm. With the increase in temperature, the sensor presented an error of + -3.5%. However, the temperature influence can be compensated and that way you obtain an error approximately of 0.9%. In another paper, Kang et al. [25] propose using an inductive sensor based on coils to measure the conductivity. The coils have a magnetic core of Mn-Zn ferrite and copper wires coiled around them. One coil is the powered coil, the other is the sense coil. The range of the prototype is between 0 and 350 mS/cm.

The use of an inductive sensor with cores presents more important problems with the temperature than sensors without it. The temperature changes the core's magnetic permeability and, therefore, changes the calibration. Though temperature can be monitored in the sewerage, the inclusion of a temperature sensor can present problems to the sewerage. In addition, these sensors have a diameter less than solenoid coils, which can facilitate clogging inside the sensor.

2.3 | Turbidity sensor

In this subsection, we present different papers proposed to monitor turbidity. Turbidity measures the water's clarity and is related to the presence of solids in the water.

One method is the use of Secchi disk. The Secchi disk is a low cost and easy method to monitor turbidity in the water bodies. It is based on introducing a disk into the water and measuring the depth at which the disk is no longer noticeable from the surface. Bigham et al. [26] collected individual Secchi disk measurements across the United States performed by volunteers and professionals in the different water bodies. They inserted this data into a database for future research and water management. One problem with this technology is that it is subjective since the person who performs the methodology sees or stops seeing the disk. In addition, the Secchi disk is very complex to automatise. Thus, other techniques have been developed to eliminate the subjective measure of turbidity and automatise it.

The most popular method used to monitor turbidity is based on optical sensors. Prerana et al. [27] proposed using optical fibre to monitor the turbidity in terms of the total interaction coefficient of light. The optical fibre comprises seven peripherical plastic cladding silica fibres to collect the light scattered in the sample. In addition, the optical fibre has a

glass core to provide light to the sample. They used a laser of 632.8 nm to irradiate the glass fibre and a mirror to reflect the light captured by the peripherical fibres. Their sensor obtained good results in low turbidity levels. Another work is presented by Yeoh et al. [28]. Their proposal is based on a pair of multimode fibres. They used a laser of 808 nm as a light source and tested 3 angles between the emitting and receiving fibre. They selected the angle of 45° because it presents the best correlation between the mathematical model and the measurements. The sensor can work between 0 and 110 NTU with a medium quadratic error of 2.38 NTU. Optical fibre can have a high cost. Therefore, other authors propose the use of LEDs as the light source. Wang et al. [29] proposed a low-cost turbidity sensor for monitoring freshwater. They used an infrared LED of 850 nm, a phototransistor at 90° to detect the scattered light, and a photodiode at 180°. These components are fixed to a transparent acrylic tube of 20 mm. The phototransistor at 90° was used in the range of 0 to 200 NTU (precision 0.1 NTU), and the photodiode at 180° was used in the range of 0 to 1000 NTU (precision 1.0 NTU). In the sewerage, we discard the photoreceptor at 180° due to the water level being variable in time. The use of a photoreceptor at 90° is not recommended because if the photoreceptor is placed inside the water, it can get dirty, and if it is placed outside the pipe, light may not reach the photoreceptor.

2.4 | Oil sensor

In this subsection, we show different studies about detecting oil in water.

The use of remote sensing is one of the methods to detect oil on large water surfaces. The use of remote sensing to monitor the presence of spills in oceans is studied by Fingas and Brown [30]. They differentiate between passive and active methods. On the one hand, the passive methods use the light reflected by the water bodies to detect the presence of oil. The light regions that can be used are (I) Visible spectrum, (II) infrared, (III) near-infrared, and (IV) ultraviolet. On the other hand, active methods are based on the emission of light or sound to detect the oil spill. The active methods are (I) Laser fluorosensors, (II) Radar, and (III) Acoustic travel time. An example of the passive method is preset by Arslan [31]. Arslan proposed the use of Sentinel 1 C-band SAR and Landsat 8 to study the oil spills. They used a real oil spill in Ildır Bay (Izmir, Turkey) on 18 December 2016. The band selected in Sentinel l1 is vertical transmission and vertical reception of radar images (VV). First, the radar image showed the possible presence of an oil spill near the ship. Then, Landsat 8 was used to validate the information. In another work, Srivastava and Singh [32] analysed the use of Moderate-Resolution Imaging Spectroradiometer (MODIS-Aqua) high-resolution bands (250 and 500 m) in Lake Maracaibo, Venezuela on 18, 19, and 20th January 2003. They concluded that radiation at 469, 555, and 645 nm atmospherically not corrected presents a good performance to detect the spill. However, the image treatment to correct the atmospherical perturbation can mask oil stains in these bands. To improve the identification of spills, the authors propose that the sum ratio of band 3 (645 nm) and band 2 (555 nm) normalised with band 1 (469 nm)' produced significant results. Remote sensing works well for large surfaces that cannot be monitored with sensors. However, it presents important gaps in small surfaces. In this paper, we will monitor the presence of oil in the sewerage. Therefore, we will not be able to use this technology.

As remote sensing is discarded on small surfaces, optical sensors are a solution. Some optical sensors have been developed to detect oil in water. Hou et al. [33] proposed the use of a sensor based on ultraviolet-induced fluorescence and fluorescence-filter systems to monitor the presence of oil in the yellow sea (China). They used a Xenon lamp (200–300 nm) as a light source, a photomultiplier tube as a light receptor, and a light filter system. The light filter system allows light to pass between 300 and 400 nm. This filter is used to increase the accuracy and reduce the noise in the photoreceptor due to the sunlight. The use of UV light can be expensive. One solution is the use of LEDs as light sources. Oh and Lee [34] studied the use of artificial light to detect the presence of oil. They tested different colour LEDs (red, green, blue, and orange) submerged at 20 mm, and they illuminated a CCD sensor located at 4 cm to the water surface. In the 4 LEDs, the blue light presents the best relationship between the increase of oil thickness and the light intensity in the CCD sensor.

In this paper, we propose a WSN to detect the presence of illegal spills in the storm sewerage and detect the presence of blockage in the sewerage. For these objectives, we use water level, rain, conductivity, oil, and turbidity sensors.

3 | DESIGN PROPOSAL

In this section, the design proposal is commented. Firstly, we analyse the scenarios with different combinations of water in the pipes and weather conditions (it rains or it does not rain). After that, the communication architecture is detailed, along with the procedures needed in the system. Then, the messages are described. Finally, the implementation details about how to read the data from the sensors are discussed.

3.1 | Scenarios

In this section, we analyse the 4 scenarios that may happen in the combination of rain and level sensors.

(I) The first scenario is when it rains and there is water in the pipe. In this condition, we use the level sensors to detect blockages in the pipes. In addition, we use turbidity, conductivity, and oil sensor to detect the presence of possible spills.
(II) The second scenario is produced when it is raining and there is no water in the pipes. This is an indication that the rainwater is not entering the sewerage. This can occur by a blockage in the storm drain.

(III) The third scenario is when it is not raining, but there is water in the pipes. The presence of water in the storm sewerage can be produced by an illicit spill or due to a discharge of a stormwater tank.
(IV) Finally, the last scenario is when it is not raining and there is no water in the pipes. In this situation, there are no more things to analyse.

3.2 | Communication architecture and algorithms

Figure 1 depicts the scheme of the communication architecture. Along the pipe, several nodes are placed to process the data obtained from the different sensors. The WSN is built using WiFi communications and the MQTT communication protocol, which will provide us with a publisher/subscriber messaging protocol that allows the nodes to send the messages described in the next subsection. These nodes are managed by the master head (MH). The MH is a special node with more computing and energy capabilities. The nodes communicate with the MH based on the data measured to ensure there are no clogs or illegal spills. Furthermore, the water tanks that collect rain have nodes to control and monitor their use.

The nodes execute a process of measurement; the pseudocode is shown in Algorithm 1. The process of measurement is constantly executed every fixed period of time, and it starts reading the level of the water. When the level is higher than a threshold, the node should start checking possible spills. This threshold could be fixed but, to allow the proposal to adapt to different pipes and scenario conditions, is statistically calculated using a p-value of 0.9. When the node starts checking the spills, the turbidity, conductivity, and oil sensors will start measuring to detect problems. In addition, the water level will be used to check if there are any clogs in the sewerage. Finally, if there is a high level in some of the measurements, these measurements will be sent to the MH along with the level measurement.

Algorithm 1. Node data processing

```
Given: threshold
level = Read_Level_Sensor()
If level > threshold
            Start_Oil_Sensor()
Start_Conductivity_Sensor()
Start_Turbidity_Sensor()
problem = Check_Oil_Problem()
    OR Check_Conductivity_Problem()
    OR Check_Turbidity_Problem()

Send_Check_Levels()
If problem
    Send_Problematics_Levels()
End if
End If
```

Figure 2 shows the process of the MH (Algorithm 2). The MH listens to messages from the different nodes. The first action is to check the level of the water. If the node has sent a level that is lower than a specific threshold (thx), the value of the raining sensor should be checked. A positive value of that sensor shows that there is a clog, since the level of water should be higher. Otherwise, there is no mismatch. If the level is higher than the threshold, the state of the water tank must be checked. If it is open or if it is closed, but it is raining, it could be a normal situation. However, if it is not, there is an illicit discharge. That could be possible even if the tank is open or if it is raining. That is the reason why the measurements are also checked in that case. When one of these problems is detected, the MH sends a message to the user. After checking is done, the MH awaits for the next message to be received.

Algorithm 2. Master head algorithm

```
    Given: refresh_time, threshold
    While true
    rain = Read_Rain()
    Read_Message_From_Node()
    If Message.level > threshold
    Send(Ask_Tank)
    Open = Read_Received_Tank()
    If NOT Open AND NOT rain
    Send_Illicit_Discharge()
    Else
    If Check_Other_Measurements()
    Send_Illicit_Discharge()
End If
    Else
    If rain
    Send_Clog()
    End If
Wait(refresh_time)
    End While
```

3.3 | Messages

The messages used in the described processes are detailed in this section. The messages that the nodes exchange in the system are the following ones:

- Ask Tank: The message is sent from the MH to a tank node. It is a request message that must be followed by a reply.
- Tank: The reply to the Ask Tank message. It indicates whether the tank is open or not.
- Measurements: This message is the one used by the nodes to send the measurements of the sensors. The size is fixed for one measurement and depending on the number of measurements sent by the node, its total size may change.

These messages are detailed in Figure 3. They follow the Type, Length, Value (TLV) scheme. Firstly, the type of the

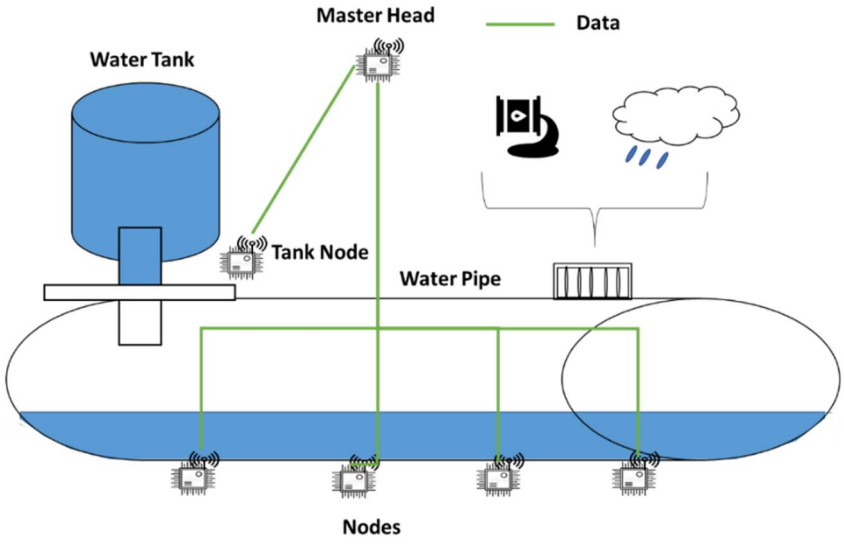

FIGURE 1 Communication architecture

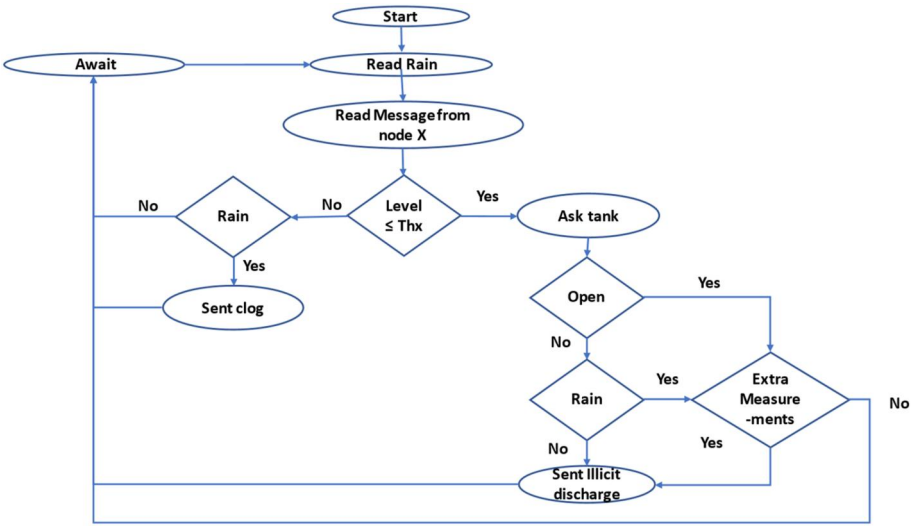

FIGURE 2 Master head algorithm

message is indicated. In this case, we have six different messages. Therefore, we need at least 3 bits to indicate the message type. Then, the length of the message is used to indicate to the receiver how many bits need to be read. Ask Tank message is empty, only the header (type and length) is needed to create the message, it needs no extra information. Therefore, only the other messages with extra data are depicted in Figure 3. The measurements message is the only one with a different structure, since the number of measurements sent by the node may change. Consequently, before each measurement, the measurement ID of the sample is needed.

3.4 | Implementation details

In this subsection, the code needed to read the data from the sensors is discussed. The implementations are designed for Atmega 2560, with the Arduino IDE.

The measurements of the different sensors are quite similar. Firstly, we have the code used to read the predicted rain in Figure 4. We used the sensor FC-37 attached to the pin 5. We use the digital value to detect, using a Boolean variable, if it is raining.

The level sensor used is HC-SR04 [35]. Like the rain sensor, the level sensor uses two pines of the microcontroller. The measurement process, using pin number 6, consists of the steps shown in Figure 5. Pin number 6 returns the time that has passed between the emission and reception of the sound. In order to get the distance, we need to multiply the time by the sound speed, but we need to divide the result because the sound covers the distance twice. Moreover, the time returned by the sensor is measured in microseconds, so we need to transform it into seconds. Then, we can print the result.

To power the system, different solutions can be implanted. The easiest solution is to connect the system with street lighting. However, in some cases, this is not an optimal

solution due to the distance of the proposed system to the street lighting or that current only passes through these cables at certain times. Other solutions includes using solar panels on surfaces or the use of batteries. The optimal solution requires further study in each case.

The conductivity, turbidity, and oil sensors are provided in previous studies. The turbidity sensor is presented in Ref. [36], the conductivity sensor is presented in Ref. [37], and the oil sensor is presented in Ref. [38].

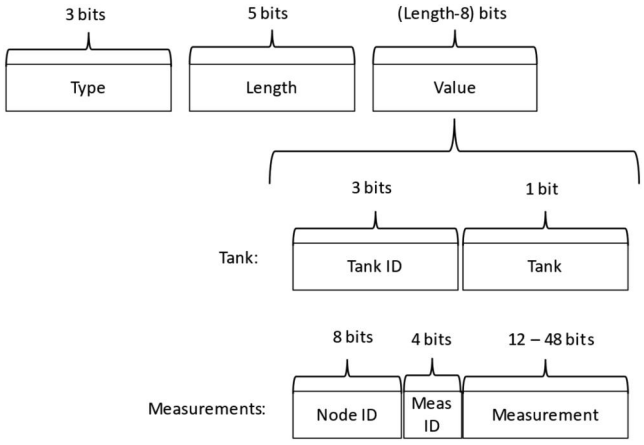

FIGURE 3 Messages used in the communication

```
boolean RAIN= false;
int pinRain = 5;
pinMode(pinRain, INPUT);
RAIN = !(digitalRead(pinRain));
if(RAIN)
   Serial.println("It is Raining");
else
  Serial.println("It is not Raining ");
```

FIGURE 4 Rain sensor data reading code

```
int pinLevel = 6;
const float SSpeed= 34000.0;
float distance  = pulseIn(PinEcho, HIGH)* 0.000001 * SSpeed / 2;
Serial.print(distance);
Serial.print("cm");
Serial.println();
```

FIGURE 5 Level sensor data reading code

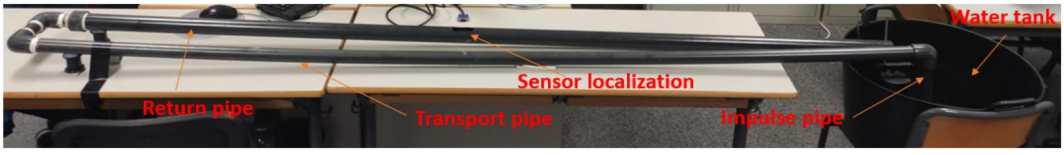

FIGURE 6 Hydraulic circuit

4 | TEST BENCH

In this section, we explain the methodology used in this paper. First, we explain the methodology used to calibrate oil and conductivity sensors. Then, we show the methodology used to check the use of level sensors in sewerage.

4.1 | Conductivity and oil sensor

In this subsection, we explain the methodology used to obtain the data of the oil and conductivity sensors.

We performed a closed hydraulic circuit with PVC pipes as presented in Figure 6. The circuit starts in a water tank with a pump for pumping water. The pump has a power of 400 W, providing a flow of 1.7 L/s. The pumped water is impulsed to the circuit through an impulse pipe. The pump pumps the water from the base of the water tank to the circuit through an impulse pipe. The impulsion pipe has a height of 25 cm. Next, an elbow connects the impulse pipe and the transport pipe. The transport pipe has a length of 2 m. Then, two elbows are connected from the transport pipe to the return pipe. The return pipe returns the water to the tank. The return pipe has a slope of 2%. The conductivity and oil sensors are placed in the middle of this pipe. The pipes used have an external diameter of 50 mm, and a thickness of 3 mm. In the two tests, we used 20 L of freshwater, and each measurement is performed in triplicate.

Conductivity and oil sensor calibration are carried out separately. First, we perform a conductivity test by adding table salt to the water to analyse the different samples. The concentration of samples used for the calibration and verification is represented in Table 1. We use a conductivity sensor presented previously in Ref. [37]. We add an epoxy layer to the sensor to increase its protection. On the one hand, the epoxy layer protects the insulating layer of copper from the chemicals that can be present in the storm sewerage. On the other hand, the epoxy helps keep the spires in the same position by keeping them glued together. The conductivity sensor is based on

2 coils with 40 and 80 spires of copper with a diameter of 0.4 mm. The powered coil is the coil with 40 spires and the other is the induced coil. The function generator model AFG1022 [39] is used to power the coil. We use an oscilloscope model TBS1104 [40] to measure the voltage induced. The powered coil has a current of 3.3 V peak to peak with a series resistance of 47 Ω. We use a metallised polyester film capacitor of 10 nF parallel to the coil in the induced coil. We test the frequencies between 150 and 180 kHz, each 1 kHz. We select these frequencies due to the frequency peak is between 160 and 170 kHz, and we want to know the behaviour of the sensor in the frequencies nearby to select the best working frequency.

Details regarding the oil sensor is available in Ref. [38]. However, we add an infrared LED and photodiode to improve the prototype. We use the same hydraulic circuit explained previously. As the sensor can be affected by the external light, we cover it with an opaque bag. When we start the measurements for each concentration, we clean the sensor. We use a multimeter model Tenma 72-2600 [41] to measure the resistance of the LDR and the output voltage (V_{out}) of the photodiode. In our design, we use a voltage divider formed by a fixed resistance and, after the circuit, the photodiode or LDR.

A power supply model FAC-662B is used to power the LEDs and photodiode. The LEDs are powered sequentially with a voltage of 5 V, and each is powered for 20 s. We want the intensity current for the colour LEDs to be close to 15 mA. We select this value because the colour LEDs are not recommended to have an intensity current higher than 20 mA. However, as we use standard resistance, the real intensity of the colour LEDs are 13.48, 13, 12.33, 13.6, and 12.39 mA to yellow, red, blue, green, and white, respectively. In the infrared LED, we test with different intensities. These are 13.2, 17.4, 23.2, 34.4, 49.6 and 90 mA. The maximum intensity recommended in the infrared LED by the manufacturer is 150 mA.

The values of resistance of the LDR must be changed to voltage to allow the microcontroller to read it. We use a voltage divider for signal conditioning. To select a fixed resistance value, we find a value to maximise the difference between the water without oil and the maximum concentration of oil tested. In the case of the photodiode, we measure the V_{out} directly. For this, we need to determine previously the resistance that we will be using. To determine it, we tested with different current intensities in the infrared LED and changed the fixed resistance. In the fixed resistance, we test with different resistances between 1 kΩ and 8.2 MΩ. To perform this test, we use the pipe with water and a black object that simulated the presence of oil. We do not use oil to determine the fixed resistance to prevent water pollution.

$$V_{out}\,(V) = V_{in}\,(V) * \frac{\text{RLDR}\,(k\Omega)}{\text{Fixed resistance}\,(k\Omega) + \text{RLDR}\,(k\Omega)} \quad (1)$$

For elaborating the different oil samples, we use the same water to reduce the quantity of polluted water. In the water, we add different volumes of oil to elaborate the sample. Once the sample is elaborated, we measure with the sensor and repeat the process for each sample. The concentrations used in the calibration and verification are represented in Table 2. We use used oil provided by a local car workshop in Valencia (Spain). The oil was used by a gasoline car for 31,000 km and 15,526 km.

4.2 | Blockage detection in sewerage

In this subsection, we explain how the simulations are performed to determine the possibility of using level sensors to monitor the sewerage.

The software used to perform the simulation is the EPA Storm Water Management Model SWMM 5.1 [42] to simulate a subsection of a storm sewerage network. The software offers different models for simulating storm sewerage. We select the dynamic wave model because this model calculates the water that accumulates in the sewer in the case of excess water. The model needs the rain values to calculate the water entering the sewerage. We create artificial rain represented in Table 3.

The measurements of the basins and pipes used in the simulation have been obtained following an industrial park's typical distribution. This distribution is large plots occupied by industrial buildings and streets for access. The storm sewerage is distributed in accordance to the streets, and the different buildings dump the pluvial water into the street. In our simulation, we have 4 plots of 4.5 ha each. Each plot is subdivided

TABLE 1 Salt concentration used in calibration and verification

Calibration	Salt (g/L)	0.0	1.0	3.0	4.0	5.0	7.0	10.0	12.0	15.0	18.0	20.0	22.0	25.0	28.0	35.0
	Conductivity (mS/cm)	0.53	2.66	6.68	8.59	10.64	14.34	19.7	23.2	28.2	32.9	36.2	39.6	44.2	48.8	58.4
Verification	Salt (g/L)	2.0		4.5		8.0		13.0		19.0		23.0		30.0		
	Conductivity (mS/cm)	4.73		9.58		16.15		24.9		34.5		41.1		51.9		

TABLE 2 Oil concentration used in calibration and verification

Calibration (mL oil/L water)	0.0	0.2	0.4	0.6	0.8	1.0	1.2	1.4	1.6	1.8	2.0	2.2	2.4	2.6	5.0	10.0	15.0	20.0	25.0	30.0	35.0	40.0	45.0
Verification (mL oil/L water)	0.1			0.7			1.3			1.9			2.5			17.0			32.0			47.0	

into six parts (sub-basins) that dump the stormwater into a node. We estimate that 90% of the area is impervious as it is an industrial zone. The rest of the parameters are the default values of the programme. The pipe diameter used is 0.5 m diameter for all pipes with a pending of 2%. These are the minimum values recommended in the storm sewerage. The simulation concept is represented in Figure 7, and Table 4 shows the values of length and heights of the different pipes.

TABLE 3 Values of the artificial rain

Time simulation (h)	1	2	3	4	5	6	7	8	9
Rain (mm)	0	7	6	8	20	7	5	2	0

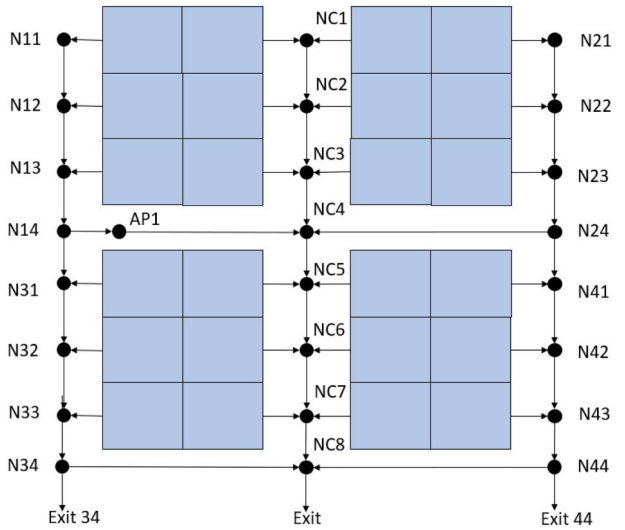

FIGURE 7 Map of the simulation section

5 | RESULTS

In this section, first, we analyse the results obtained in the oil sensor. Then, we present the results obtained in the water level simulation. Finally, we show the results of the conductivity sensor.

5.1 | Oil sensor

In this section, we show the results obtained with the oil sensor. First, we need to determine the fixed resistance in the photodiode circuit and the current intensity of the infrared LED. Then, we analyse the results obtained by the photodiode of the prototype. Finally, we study the results obtained with the LDR.

Concerning photodiode, we test with the intensity current of the infrared LED and the fixed resistance of the voltage divider. The V_{out} difference between water and the black object is represented in Figure 8. In this figure, we observe that the V_{out} difference is near 0 V in the lower fixed resistances in all intensities tested. The V_{out} difference between the water and the black object increases with the increase in resistance up until a maximum. To the intensities of 49.6 and 90 mA, the maximum difference occurs at 2.2 MΩ. With the increase of the fixed resistance, we observe a reduction of the V_{out} difference in these two current intensities, which would indicate a parabolic behaviour with the increase of fixed resistance. In the other intensities tested, we do not observe a maximum. We think that these intensities with the increase of the resistance in the circuit probably have the same behaviour as the intensities 49.6 and 90 mA. However, we did not test higher resistance values because these are not standard values, and we discarded the idea to use more than one resistance to facilitate the use of the sensor. In the resistance of 2.2 MΩ, the V_{out} difference is

TABLE 4 Values of length and heights of the different pipes

Pipe	Length (m)	Start height (m)	Finish height (m)	Pipe	Length (m)	Start height (m)	Finish height (m)
NC1-NC2	93.3	11.4	9.5	N22-N23	93.3	12.7	10.9
NC2-NC3	93.3	9.5	7.7	N23-N24	93.3	10.9	9.0
NC3-NC4	93.3	7.7	5.8	N24-N41	5.0	9.0	8.9
NC4-NC5	5.0	5.8	5.7	N24-NC4	160.0	9.0	5.8
NC5-NC6	93.3	5.7	3.8	N31-N32	93.3	8.9	7.0
NC6-NC7	93.3	3.8	2.0	N32-N33	93.3	7.0	5.2
NC7-NC8	93.3	2.0	0.1	N33-N34	93.3	5.2	3.3
NC8-Exit	5.0	0.1	0.0	N34_Exit34	5.0	3.3	3.2
N11-N12	93.3	14.6	12.7	N34-NC8	160.0	3.3	0.1
N12-N13	93.3	12.7	10.9	N41-N42	93.3	8.9	7.0
N13-N14	93.3	10.9	9.0	N42-N43	93.3	7.0	5.2
N14-NC4	160.0	9.0	5.8	N43-N44	93.3	5.2	3.3
N14_N41	5.0	9.0	8.9	N44-NC8	160.0	3.3	0.1
N21-N22	93.3	14.6	12.7	N44-Exit44	5.0	3.3	3.2

0.21, 0.39, 0.43, 0.39, 0.87, and 0.89 V to an infrared intensity current of 13.2, 17.4, 23.2, 34.4, 49.6, and 90 mA, respectively. In the same intensity currents and the change to fixed resistance to 8.2 MΩ, the difference of V_{out} is 0.52, 1.03, 1.06, 0.98, 0.76, and 0.00 V, respectively. The maximum difference is produced at the infrared LED intensity of 23.2 mA with a resistance of 8.2 MΩ. We determine that is the best option because it is the option with a greater V_{out} difference and the intensity current is not high.

With the intensity of the infrared LED and the fixed resistance determined in the photodiode's voltage divider, we start the test in the different oil samples. In Figure 9, we can observe the V_{out} obtained in the different lights used with a photodiode as photoreceptor. The V_{out} obtained is low in the green, blue, yellow, and red lights. We discard these lights to monitor the oil in the sewerage with the configuration tested. In the case of white light, we observe a few increases of the V_{out} with the increase of oil concentration. This increase is 0.29 V between 0 and 45 mL oil/L water. The increase of V_{out} is produced mainly between the concentrations of 0 to 2.6 mL oil/L water. In this range, the difference of V_{out} is 0.13 V. This difference is too little, and we must rule out white light with the photodiode as photoreceptor. Finally, there is a difference of V_{out} of 2.17 V in the use of infrared light between the water without oil and the maximum mix of water and oil tested. With the use of the infrared LED, we observe three trends. In the first trend, the V_{out} increases in the range of 0 to 1 mL oil/L water. The second trend is detected in 1 to 5 mL oil/L water, where the V_{out} is constant. Finally, there is another trend in 5 to 45 mL oil/L water, where the V_{out} increases. The infrared LED is the only one that we can use to monitor the presence of oil with a photodiode in our prototype. In future works, we will use other configurations of intensities and fixed resistance to check if the other lights can be used with a photodiode to monitor the presence of oil in the sewerage.

Now, we analyse the mathematical models that relate the V_{out} with the oil concentration. We use Statgraphics software [43] to calculate the models. We use one model for all oil concentrations tested represented in Equations (2), and two models for the low oil concentration, and the other for the high oil concentrations represented in Equations (3) and (4). The values of R2, absolute error, and relative error of these

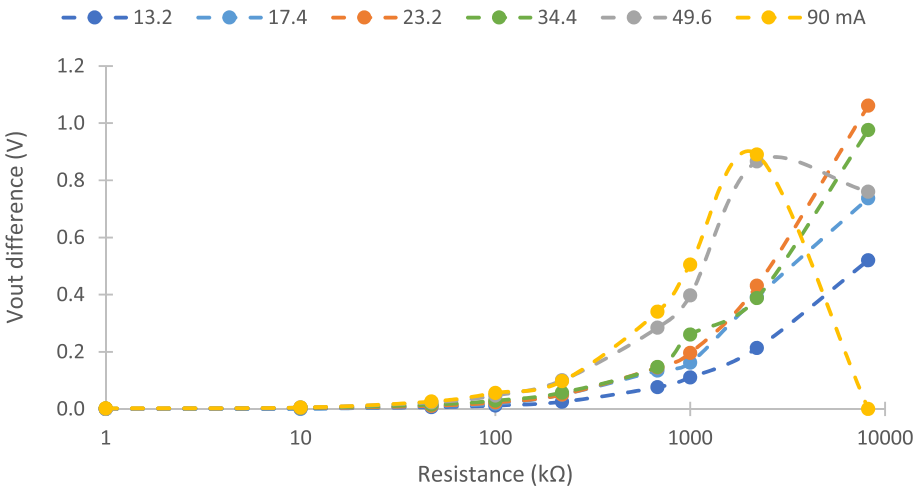

FIGURE 8 Effect of the intensity and fixed resistance in the voltage divider in V_{out} difference

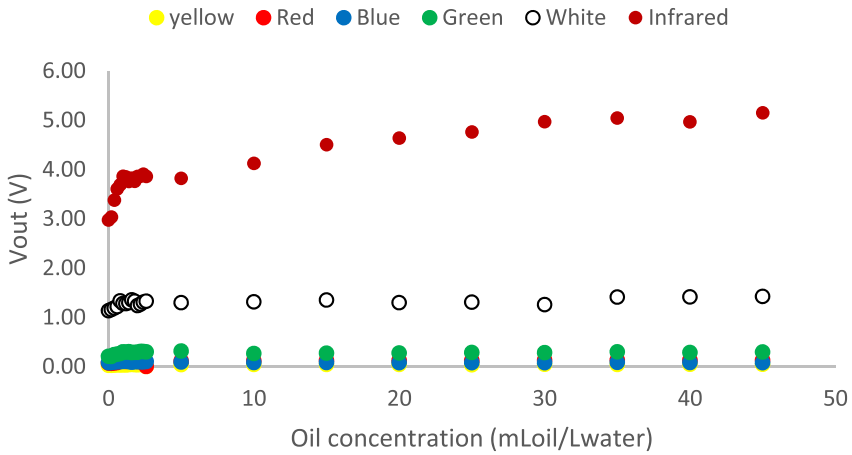

FIGURE 9 V_{out} with the use of photodiode in the different oil concentrations

models can be observed in Table 5. Using one model for all the oil concentrations, the absolute error is 1.5 mL oil/L water with a relative error of 47.7%. In this model (Equation 1), the maximum relative errors are produced in the range of 0 to 10 mL oil/L water. In this range, the mean of relative error is 66.73%. We consider these relative errors too high for our sensor. For this motive, we decided to use two models. On the one hand, a model in the concentrations between 0 and 2.6 mL oil/L water. The absolute error of this model is 0.3 mL oil/L water, and the relative error is 31.3%. On the other hand, the second model (5 to 45 mL oil/L water) has an absolute error of 2.1 mL oil/L water and a 9.8% relative error. The use of two models reduces the errors. However, the errors in the low oil concentrations are too elevated. In Figure 10, we represented the observed versus predicted values using the model in the range of 0–2.6 and 5 to 45 mL oil/L water. In Figure 10a, we observe the low concentration of oil values. In general, we confirm that the mathematical model is ineffective in predicting oil concentration. Nevertheless, in the high concentration of oil tested (Figure 10b), we can regard that the model predicted well the concentration of oil.

$$\text{Oil concentration}\left(\frac{\text{mL oil}}{\text{L water}}\right) = \left(-4.20311 + 0.400849 * V_{\text{out}}{}^{2}\right)^{2} \quad (2)$$

$$\text{Oil concentration}\left(\frac{\text{mL oil}}{\text{L water}}\right) = \left(-1.62013 + 0.198401 * V_{\text{out}}{}^{2}\right)^{2} \quad (3)$$

$$\text{Oil concentration}\left(\frac{\text{mL oil}}{\text{L water}}\right) = \left(-3.18522 + 0.3644 * V_{\text{out}}{}^{2}\right)^{2} \quad (4)$$

Finally, we perform a verification of the sensor. In the range of 0 to 2.6 mL oil/L water, the absolute error is 0.77 mL oil/L water, and the relative error is 63.39%. With the errors observed in the calibration and verification, we can affirm that the sensor cannot be used to determine the oil concentration in this range. However, we think that the sensor can be used to determine the presence of oil. In the range of 5–45 ml oil/L water, the average absolute error is 3.16 mL oil/L water, and the relative error is 11.23%. The relative error is 12.84%, 16.77%, and 4.08% in the concentration of 17, 32, and 47 mL oil/L water, respectively. In this case, we can affirm that the sensor can be used to monitor the oil concentration in the range of 5 to 45 mL oil/L water. Thus, we can use infrared light with a photodiode as photoreceptor to detect the presence of oil in low concentrations and quantify the concentration in higher concentrations. Now, we study the values obtained with the LDR. The resistance values of the LDR in the use of the different lights are transformed to voltage using Equation (1). First, we search for the fixed resistance value that maximises the difference between the minimum and maximum V_{out} values. Usually, the resistance values obtained with this method are not standard. Thus, we select the standard resistance value nearest to it. Table 6 represents the calculated resistance value and the standard resistance value used.

Once the resistance values are transformed to V_{out}, we obtained Figures 11 and 12. Figure 11 represents the values

TABLE 5 Values of R2, errors, and range of the different equations

Equation	Range	R2	Absolute error (mL oil/L water)	Relative error (%)
2	0–45	0.9549	1.5	47.7
3	0–2.6	0.8353	0.3	31.3
4	5–45	0.9643	2.1	9.8

TABLE 6 Values of resistance in the fixed resistance

Colour	Yellow	Red	Blue	Green	White	Infrared
Model resistance (kΩ)	81.55	21.57	94.03	7.87	5.52	9716.02
Standard resistance (kΩ)	82.0	22.0	100.0	8.2	5.6	10,000

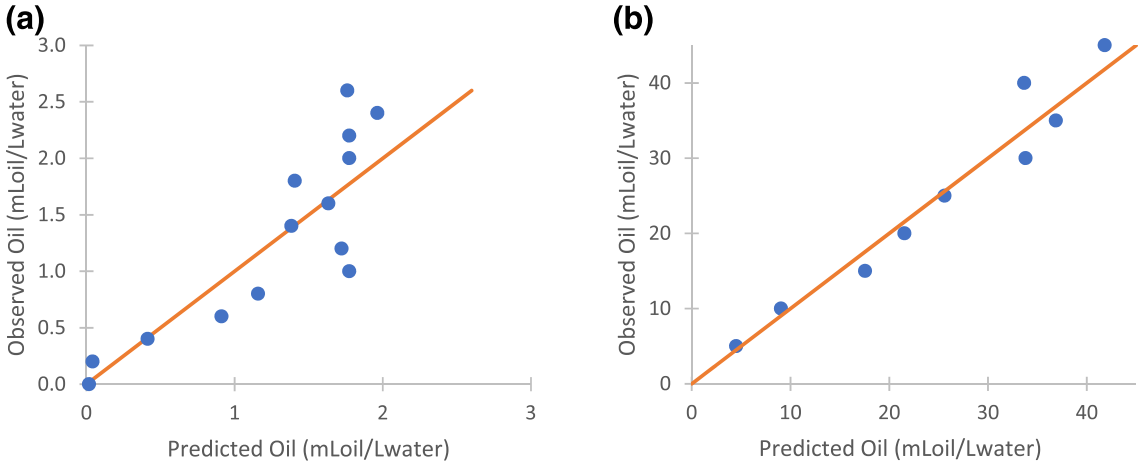

FIGURE 10 Two models

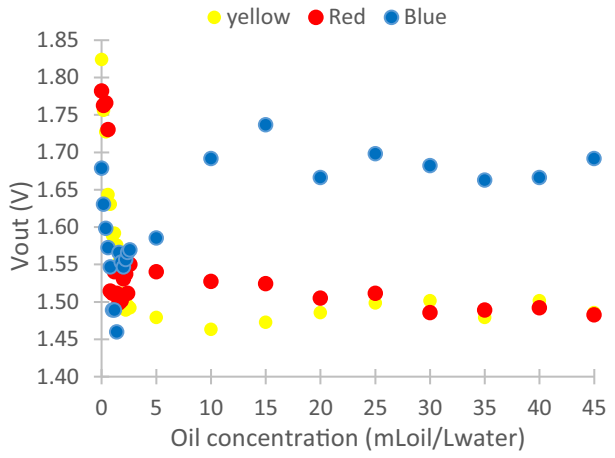

FIGURE 11 V_{out} in the different oil concentrations whit the use of yellow, red, and blue lights

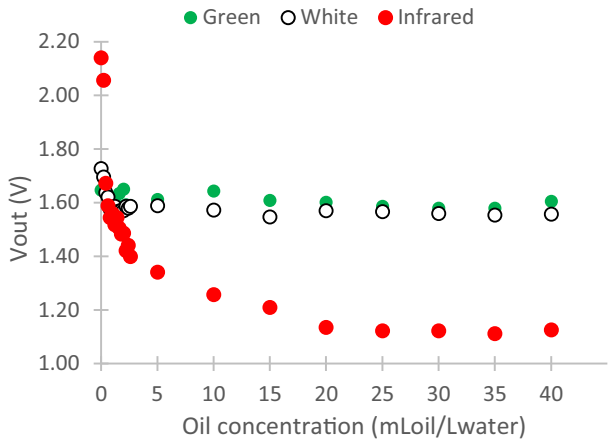

FIGURE 12 V_{out} in the different oil concentrations whit the use of green, white, and infrared lights

of V_{out} with the use of the light colours yellow, red, and blue. With the use of yellow and red lights, there is a decrease in the V_{out} with the increase of the oil concentration. The decrease of V_{out} with the yellow light is 0.36 V between the minimum and maximum oil concentration tested. The decrease is produced between 0 and 1.8 mL oil/L water. In the higher concentration tested, the V_{out} has similar values with a limit lower than 1.46 V. With red light, the V_{out} decrease is 0.3 V between the water without oil and the water with the maximum oil concentration. In this light, the V_{out} decrease is produced mostly in the concentration between 0.6 and 0.8 mL oil/L water. Thus, we discard the use of this light to monitor oil concentration. However, this light can be used to differentiate between water with oil and water without oil. Another light tested is the blue light. The evolution of V_{out} with the oil concentration is not consistent. First, there is a V_{out} reduction up until 1.4 mL oil/L water concentration. From this concentration up until the concentration of 15 mL oil/L water, there is an increase of the V_{out} with the increase of oil concentration. In higher concentrations than 15 mL oil/mL water, the V_{out} trends to an upper limit of 1.73 V. The other lights tested (green, white, and infrared) are represented in Figure 12. About these lights, we discard the use of green and white lights. Because the difference of V_{out} is little when considering the increase of oil. In the use of green light, the V_{out} has values between 1.58 and 1.65 V. With the use of white light, the V_{out} without oil is 1.55 V, and the V_{out} with the maximum tested oil is 1.73 V. This is a decrease of 0.28 V that is produced mainly between the concentrations of 0 to 0.8 mL oil/mL water. In higher concentrations, we observe a low limit of 1.55 V. Finally, we analyse the use of infrared light. With this light, there is a decrease of the V_{out} of 1.03 V between the water without oil and the maximum oil concentration tested. As in the previous cases, the values of V_{out} have a lower limit of 1.12 V as of 20 mL oil/L water. The reduction of the V_{out} is indicative of the increase of light that hits the LDR. This can increase the light reflected by the water of oil or fluorescence produced by one or more substances present in the oil. In future works, we will test which of these effects are the most predominant to improve the sensor.

Given the previous results, white and red light can be used to detect the presence of oil but not for monitoring. The yellow and infrared light are useful for monitoring the oil concentration in different ranges. The yellow light can be used in 0 to 2.2 mL oil/L water, and infrared light in the range of 0 to 20 mL oil/L water. First, we analysed the results obtained with the yellow LED. Equation (5) represents the mathematical model that related the oil concentration with the V_{out} in this light. The value of R2 of the model is 0.97293, and in Figure 13, the predicted values versus the observed values of the model are represented. In general, the values obtained from the model predicted the observed values well. We do not observe an important difference between the observed and predicted oil concentrations.

$$\text{Oil concentration}\left(\frac{\text{mL oil}}{\text{L water}}\right) = \left(4.23337 - 1.24727 * V_{out}\ \text{yellow}^2\right)^2 \quad (5)$$

Now, we analyse the models of V_{out} with infrared light. First, we calculate the mathematical model with Statgraphics [43] with the V_{out} values between 0 and 20 mL oil/L water. We obtain Equation (6), which has an R2 value of 0.8665. This low value of R2 implies a short ability to predict the values of oil concentration. This is observed in Figure 14a,b we can see that the predicted values are far from the observed. It can be seen that the predicted value except in 0.2 and 5 mL oil/L water concentrations are far from the observed. In addition, in Table 7, the errors in the calibration and verification of that model are represented. The absolute error in the calibration is 1.2 mL oil/L water, and the relative error is 42.3%. In the verification, the relative error is similar, with 45.95%. These errors are not good for our sensor to know the oil concentration. Thus, we test with the elimination of values of the calibration. By eliminating the calibration of the value without oil, we obtained an R2 value of 0.8764. This is still a low value of R2 with which we continue to eliminate the next value of

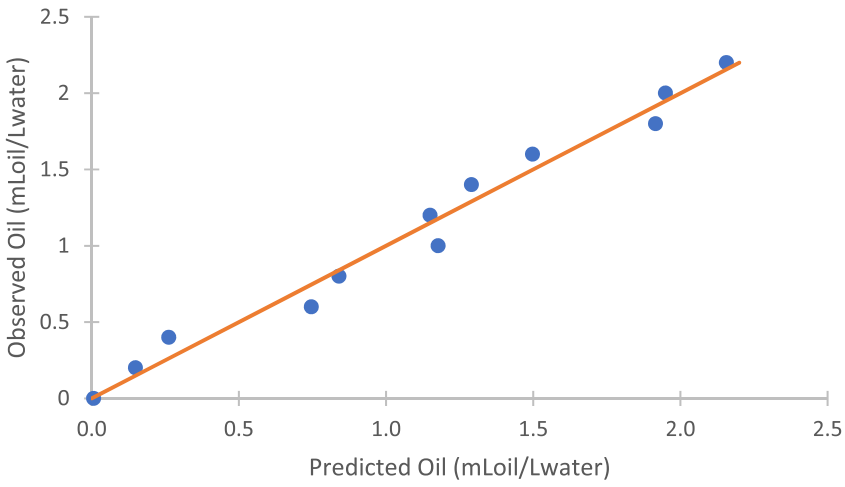

FIGURE 13 Observed versus predicted concentration of oil in yellow light

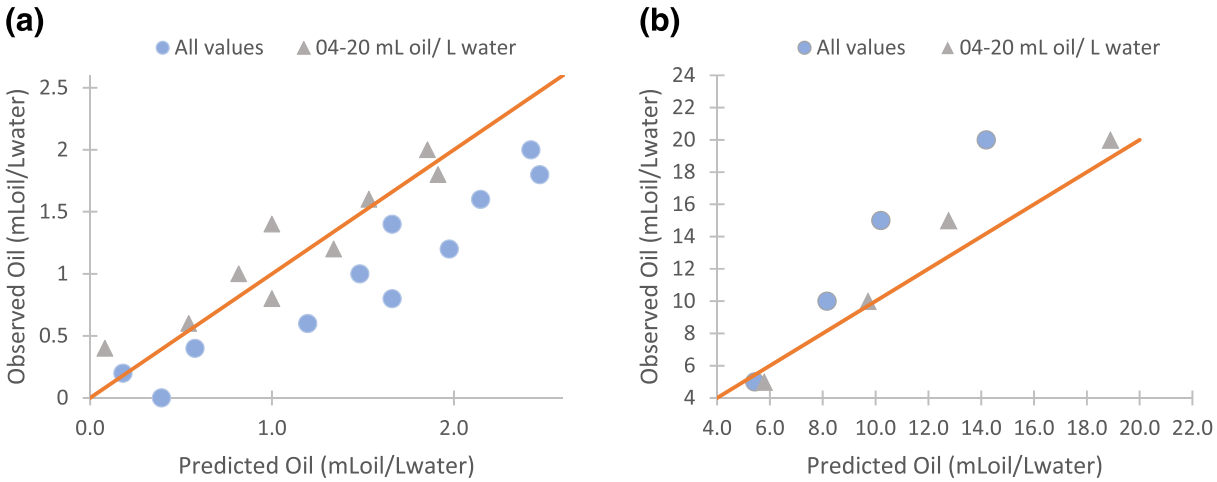

FIGURE 14 Observed versus predicted concentration of oil in infrared light in the two models

the calibration. In this case, we obtain Equation (7) with an R2 value of 0.9710 in the range of 0.4 to 20 mL oil/L water. We obtained a reduction in the errors. The absolute and relative errors are 0.54 mL oil/L water and 21.25%, respectively, in the calibration and in the verification are 1.75 mL oil/L water and 18.41%.

$$\text{Oil concentration}\left(\frac{\text{mL oil}}{\text{L water}}\right) = \left(-5.58178 + \frac{10.605}{V_{\text{out}}\ \text{infrared}}\right)^2 \tag{6}$$

$$\text{Oil concentration}\left(\frac{\text{mL oil}}{\text{L water}}\right) = \left(-8.27867 + \frac{14.3223}{V_{\text{out}}\ \text{infrared}}\right)^2 \tag{7}$$

In summary, the use of a photodiode is only effective with the use of infrared light to detect the oil concentration in the range of 5 to 45 mL oil/L water. With the use of an LDR as photoreceptor, red light can be used to determine the presence of oil, but not to determine the concentration. Regarding the yellow and infrared light, these can be used for monitoring the oil concentration. Yellow light can be used in the range of 0 to 2.2 mL oil/L water and infrared light in the range of 0.4 to 20 mL oil/L water. Infrared light is also used in the determination of turbidity.

In future works, we will study the use of artificial intelligence to detect if the answer of the sensor is due to the presence of oil or turbidity with the use of more lights. We determine that the maximum concentration that our sensor can measure is 20 mL oil/L water, using infrared light.

5.2 | Level sensor

In this subsection, we analyse the effect of the presence of a blockage or illegal spills on the water level of storm sewerage.

First, we check if it is possible to detect the presence of dumping with the use of the level sensor. Nevertheless, we do not observe a significant difference in the sewerage between the rain with a spill and no spill. This is because if we calculated

the water that enters the sewerage with the first value of rain (7 mm), we obtained 52.5 m^3/h in each node. We consider that such high volumes would not be reached in the event of an illegal discharge. Therefore, it is impossible to detect a spill with the use of level sensors at the time when rain occurs.

Now, we analyse the use of the level sensors to detect blockage in the pipes. Figure 15 represents the pipes that presented differences between a blockage and no blockage with the different percentages of blockage levels. In Figure 15a, we represent a blockage effect between one of the lateral pipes and the central pipes. If the blockage is located in the lateral pipe, we obtain the results observed in Figure 15b. We show similar pipes affected (except pipe N34 to NC8). Figure 15c and 11 D) represent what occurs if the blockage is located at the end of the simulated section. In the case of the blockage located in the lateral pipe, we observe that the pipes near the blockage are affected. However, many pipes are affected if the blockage is in the central pipe. We can affirm that the use of a level sensor can be a tool to detect the presence of a blockage.

In future works, we will test our proposal in real conditions. In real conditions, we will have the water level of the

TABLE 7 Range and errors

		Calibration		Verification	
Colour light	**Range (mL oil/L water)**	**Absolute error (mL oil/L water)**	**Relative error (%)**	**Absolute error (mL oil/L water)**	**Relative error (%)**
Yellow	0–2.2	0.09	12.42	0.21	28.65
Infrared	0–20	1.20	42.30	0.68	45.95
Infrared	0.4–20	0.54	21.25	1.75	18.41

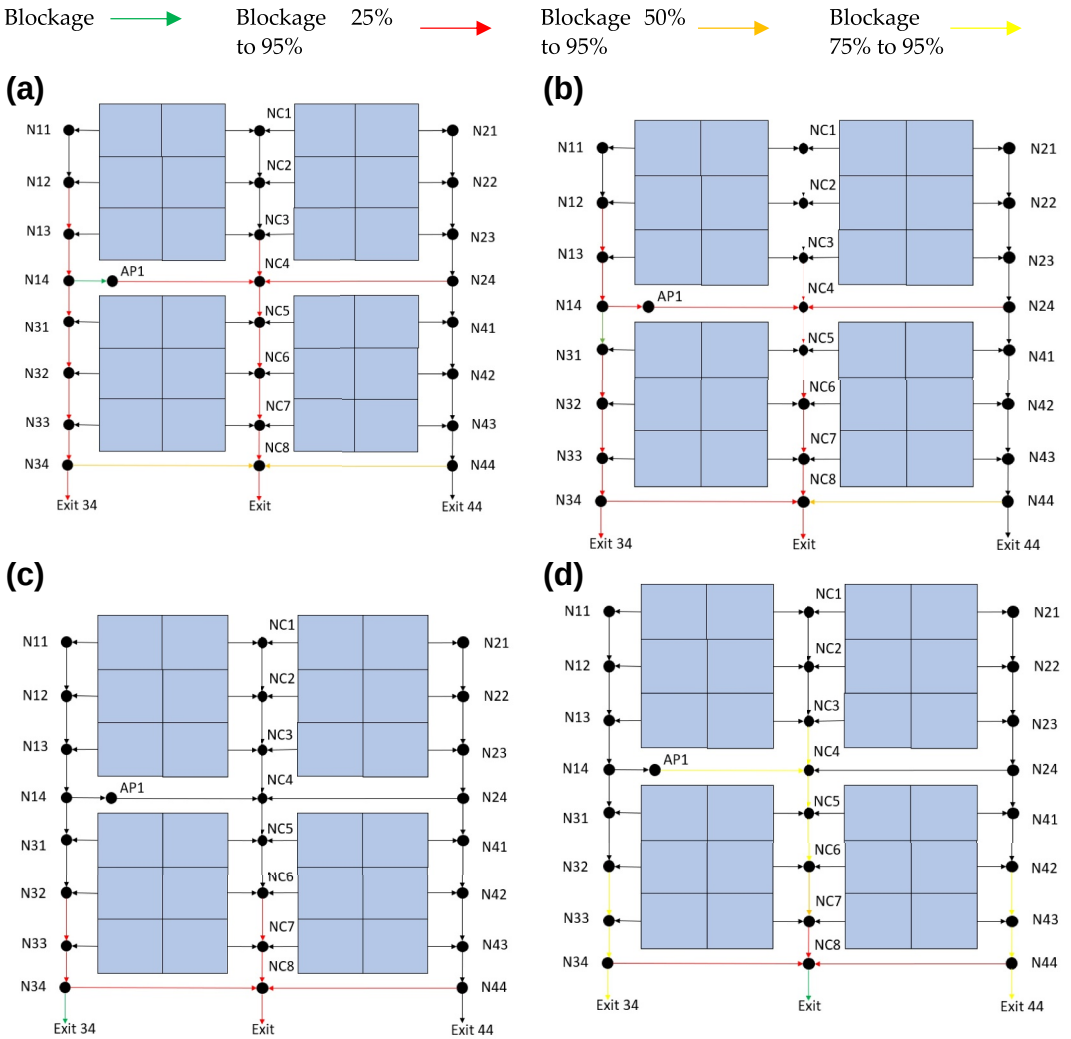

FIGURE 15 Pipes affected by the different % of blockages and blockage positions

pipes and the amount of precipitation. To determine the presence of blockage, we will use the water level values and the relation between the different water levels of the pipes using neural networks.

In sewerage, the blockage can be produced by the deposit of solids (wet wipes, rocks, trash, branches, etc.). The presence of these elements will affect the velocity of the water. Therefore, there will be an increase in water level upstream and a decrease downstream. However, a water level sensor could not detect the damage to the pipes at the top of it by the roots of trees. In future works, we will study the use of other sensors to detect the damage to pipes. Different solutions, such as the use of ultrasounds, can be explored.

5.3 | Conductivity sensor

In this section, we analyse the results obtained with the conductivity sensor.

We observe that the frequency peak changes with the increase of conductivity. The peak frequency in freshwater is 164 kHz, and the conductivity of 58.4 mS/cm is at 162 kHz.

In Figures 16–19, the values of induced voltage are represented in the different frequencies tested. We identify 4 types of trends that are represented in the different figures. The first trend is represented in Figure 16. This trend is produced between the frequencies of 150–158 kHz. First, with the increase of the conductivity, there is an increase of the induced voltage until a certain conductivity. After this conductivity, the value of induced voltage is reduced with the increase of the conductivity. In addition, we observe that the conductivity value where the change occurs between the increase and decrease of the induced voltage is reduced. Until the frequency of 159 kHz, where the voltage increases between the first and second concentration tested and then decreases with the increase in conductivity. We can see this trend in the frequencies 159–165 kHz, and the induced voltage of these frequencies is shown in Figure 17. In these frequencies, some induced voltage values can be associated with two conductivity values of water. For this reason, we discard the use of frequencies between 150 and 165 kHz. Figure 18 represents the frequencies between 166 and 176 kHz. In these frequencies, we observe an induced voltage decrease with increasing conductivity. These frequencies can be used to monitor the conductivity of the water. Finally, in Figure 19, there is a decrease in induced voltage with the conductivity increase. Except in the case of 2.66 to 6.68 mS/cm, where there is an increase in the induced voltage.

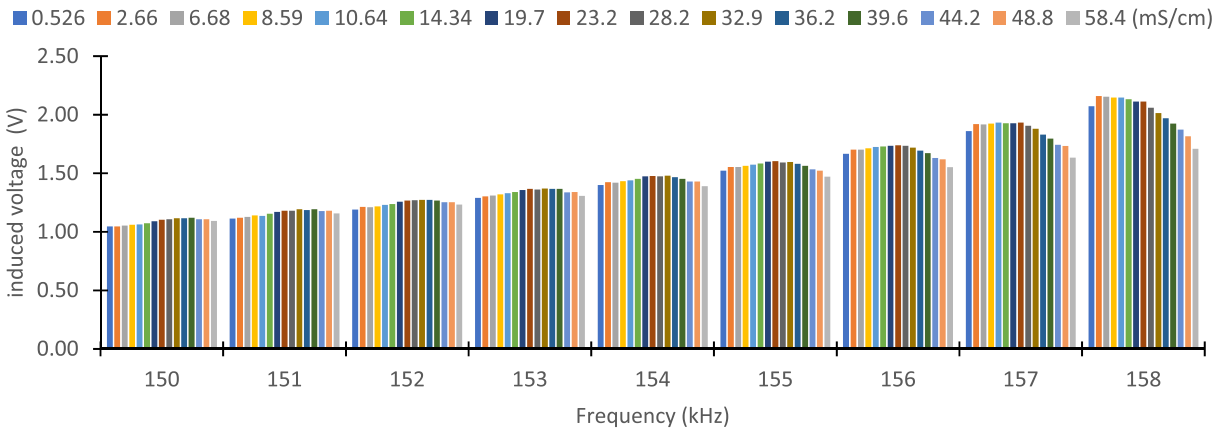

FIGURE 16 Induced voltage in the different conductivities in the frequencies between 150 and 158 kHz

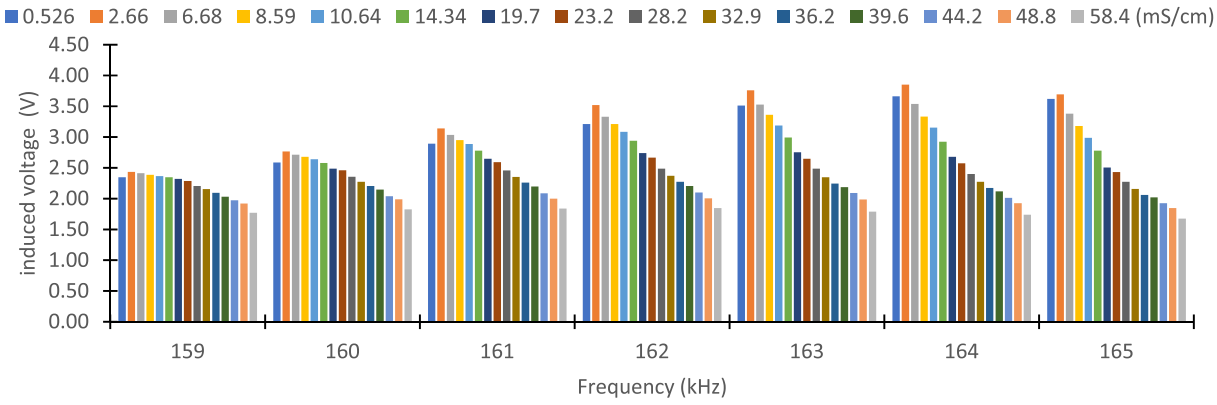

FIGURE 17 Induced voltage in the different conductivities in the frequencies between 159 and 165 kHz

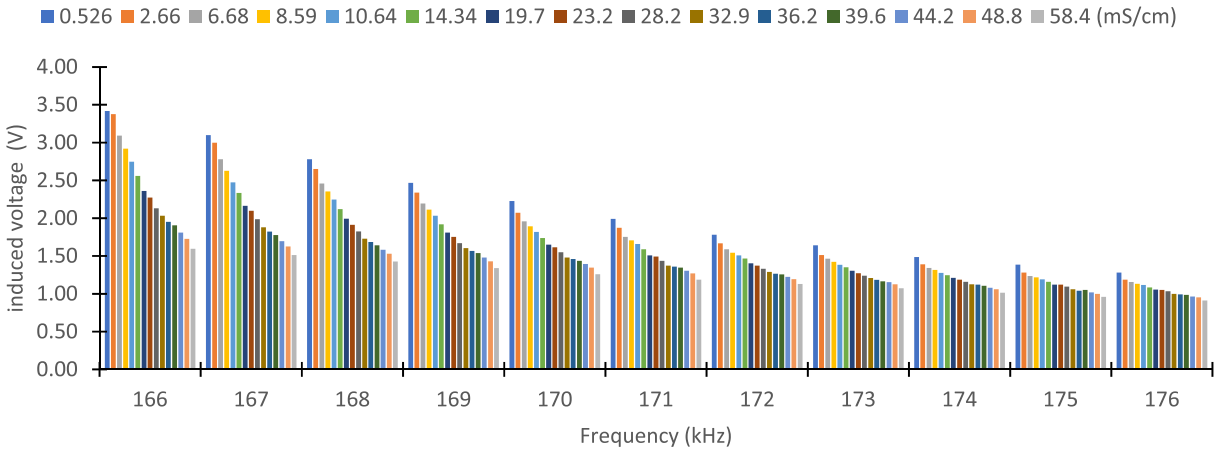

FIGURE 18 Induced voltage in the different conductivities in the frequencies between 166 and 176 kHz

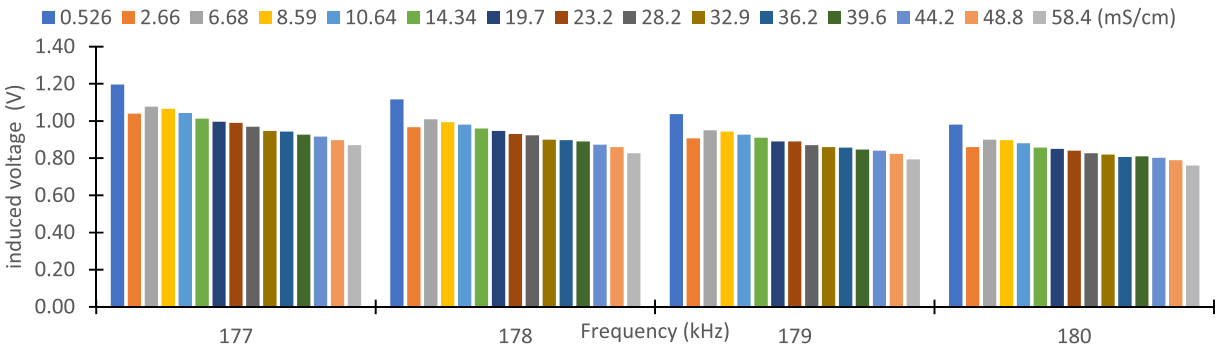

FIGURE 19 Induced voltage in the different conductivities in the frequencies between 177 and 180 kHz

The frequencies between 166 and 176 kHz are utilised to perform a calibration model. The other frequencies present changes in the trend of the induced voltage with the conductivity. This creates difficulty in the implementation of the system since an induced voltage value would be associated with more than one conductivity value. In addition, we discard the use of the frequencies 174, 175, and 176 kHz due to presenting a low induced voltage difference with the increase of conductivity.

With the data gathered of the induced voltage of the frequencies between 166 and 173 kHz, we perform mathematical models that relate the induced voltage and the water conductivity. First, we obtained the values of R2 for all models that statgraphics [43] calculated. Second, we calculate the mean of R2 for the different models in the different frequencies. Finally, we use the six models with the higher R2 mean value to relate the induced voltage with the conductivity. The models used are Square Root-Y Log-X, Square Root of Y, Inverse Y-Square Root of X, In-verse of X, Square Root-X Square-Y, and Logarithm of X. Of the six models used, the minimum error in calibration, verification or mean of calibration and verification are produced in the three first models for the relative error. The model with the least absolutive error is Square Root-Y Log-X in all cases. In Figure 20, we represent the relative error with the use of the mathematical models obtained with Statgraphics software [43]. In general, we observe that the increase of frequency reduces the relative errors (except in the case of 173 kHz).

In Figure 21, we represent the distribution of the relative errors for the different conductivity tests and frequencies selected. The model used in each frequency has fewer relative errors for that frequency. In general, the maximum relative errors are in the lower concentrations tested. The minimum relative error in the concentration of 0.526 mS/cm is in the frequency of 172 kHz with a relative error of 2.1%. The maximum error in this concentration is in the frequency of 127.3 mS/cm. In the 2.66 mS/cm concentration, the mean relative error is 22.6%, with a minimum value of 0.3% to the concentration of 171 kHz. In Figure 22, the relative error of the verification in the frequencies between 166 and 170 kHz, the relative errors are higher than the 13.1% in the other frequencies, and the relative errors are less than 5.3% are represented. In the other concentrations, the values are less than 9.1% of relative errors.

As we saw previously, the absolute Voltage difference and the total relative error are reduced with the increase of frequency. In our case, the best option is the frequency of 171 kHz. Because it is the frequency with smaller relative errors at lower conductivity concentrations, which will be the most typical concentrations in a sewer. At higher concentrations, the errors will be higher than at other frequencies, but our goal is to detect the presence of a spill. The thing that

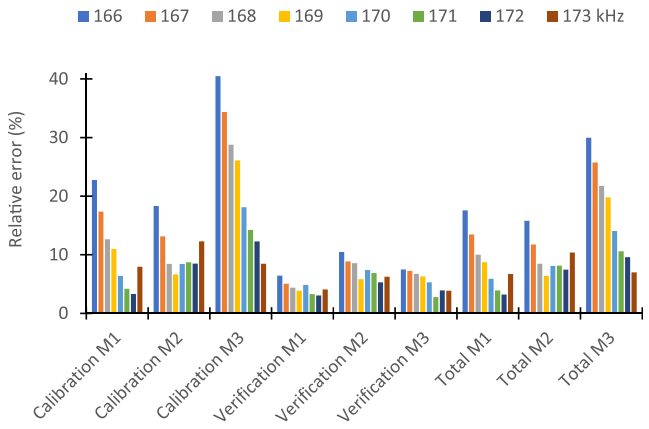

FIGURE 20 Relative errors of models

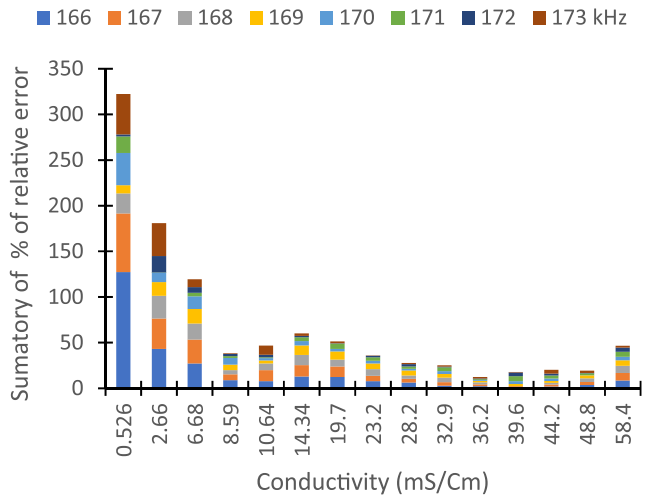

FIGURE 21 Summary of the % of relative error in the calibration

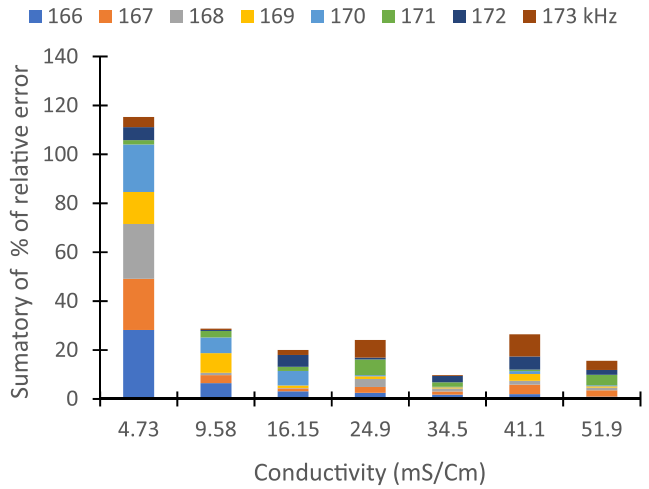

FIGURE 22 Summary of the % of relative error in the verification

would be fulfiled in that frequency. Equation 8 related the value of voltage with the oil concentration of the frequency 171 kHz,

$$\text{Conductivity mS/cm} = (10.1752 - 13.6081 * \text{LN}(V_{\text{out}}))^2 \quad (8)$$

6 | CONCLUSIONS

In this paper, we present a system to monitor the storm sewerage to prevent illicit discharges and detect blockages. Our system is composed of five different sensors (rain, water level, turbidity, conductivity, and oil) and nodes. In our system, we use two types of nodes. These are the nodes distributed in the sewer and the MH. The nodes distributed in the sewerage have oil, conductivity, turbidity, and water level sensors. These nodes communicate with the central node MH with more computational capacity and a rain sensor.

With rain and water level sensors, we established four scenarios possible. There are two options when there is water in the sewerage, but it is not raining. (I) A stormwater tank is being emptied, or (II) There has been a spill in the sewerage. In this scenario, our system checks if the stormwater tank is emptying. If the answer is negative, the sensors are used to detect who is responsible. Another scenario is when it is raining, but there is no water in the sewerage. This is a signal of the presence of a blockage in the sewer manhole. The third scenario is when there is no water in the storm sewerage and it is not raining. That is a normal situation. Finally, if it is raining and there is water in the sewerage, a spill is produced. However, only using a level sensor will not be enough to detect it. For this reason, the use of oil, turbidity, and conductivity sensors is needed. In addition, the use of the level sensor can help detect blockage in the sewerage. We tested that there are significant differences in the water level in one sewerage depending on the presence or not of a blockage.

We improve the design of two sensors previously developed: the conductivity sensor and the oil sensor. In this case, we include infrared light and a photodiode in the design previously developed. On the one hand, we obtained that infrared light and the use of a photodiode present an absolute error of 2.1 mL oil/L water in the range of 5 to 45 mL oil/L water and a relative error of 9.8%. The relative error is 11.23% in this range and 0.77 mL oil/L water of absolute error. With the use of the photodiode, the other colours of light are not useful for detecting the oil. On the other hand with the use of an LDR as a photoreceptor, red light can differentiate between water with oil and without. Regarding the yellow light, it can be used in the range of 0 to 2.2 mL oil/L water with an absolute error of 0.09 mL oil/L water. With this photoreceptor, the infrared light presents an absolute error of 0.54 mL oil/L water in the range of 0.4 to 20 mL oil/L water.

Also, we improve the design of the conductivity sensor previously developed. We detect 4 different trends of induced voltage with the increase of conductivity. The frequencies that are utilised for monitoring the conductivity are included in the range of 166–173 kHz. In general, we detect that the relative errors decrease with the increase of conductivity. In addition, the relative errors decrease with the increase of the frequency.

We select 171 kHz as the better option of measurement in this sensor. This frequency presents an absolute difference of 0.81 V in Alternating current (AC), 0.57 V in Direct current (DC) and a relative error of 3.9%.

Our WSN is useful to prevent the illicit discharge of the industrial areas in the storm sewerage.

In future works, we will analyse the use of turbidity sensors in our system. We will improve the design of the photodiode circuit to try to use other lights apart from infrared. Finally, we would like to test our combined and sanitary sewerage proposal.

ACKNOWLEDGEMENTS

This research was funded by by the Ministerio de Educación, Cultura y Deporte, through the "Ayudas para contratacion predoctoral de Formación del Profesorado Universitario FPU (Convocatoria 2016)" grant number FPU16/05540; the "Ministerio de Ciencia e Innovación" through the Project PID2020-114467RR-C33 and by "Ministerio de Agricultura, Pesca y Alimentación" through the "proyectos de innovación de interés general por grupos operativos de la Asociación Europea para la Innovación en materia de productividad y sostenibilidad agrícolas (AEI-Agri)", project GO TECNOGAR. This study also forms part of the ThinkInAzul programme and was supported by MCIN with funding from European Union NextGenerationEU (PRTR-C17.I1) and by Generalitat Valenciana (THINKINAZUL/2021/002).

INSTITUTIONAL REVIEW BOARD STATEMENT

Not applicable.

CONFLICTS OF INTEREST

The authors declare no conflict of interest.

INFORMED CONSENT STATEMENT

Not applicable.

DATA AVAILABILITY STATEMENT

The data presented in this study are available on request from the corresponding author. The data are not publicly available due to privacy constraints.

ORCID

Javier Rocher https://orcid.org/0000-0003-0182-1671
Albert Rego https://orcid.org/0000-0001-7187-6809
Jaime Lloret https://orcid.org/0000-0002-0862-0533
Luís M. L. Oliveira https://orcid.org/0000-0001-9412-5012

REFERENCES

1. Greater lansing regional committee for stormwater management (GLRC): "the different types of stormwater sewers | mysite". https://www.mywatersheds.org/the-different-types-of-stormwater-s. Accessed April 2021
2. United Nations: Water and Sanitation - United Nations Sustainable Development. https://www.un.org/sustainabledevelopment/water-and-sanitation/. accessed April 2021
3. Xu, Z., et al.: Urban river pollution control in developing countries. Nat. Sustain. 2(3), 158–160 (2019). https://doi.org/10.1038/s41893-019-0249-7
4. Rehman, F., Cheema, T.: Effects of sewage waste disposal on the groundwater quality and agricultural potential of a floodplain near Jeddah, Saudi Arabia. Arabian J. Geosci. 9(4), 307 (2016). https://doi.org/10.1007/s12517-016-2340-y
5. Zgheib, S., Moilleron, R., Chebbo, G.: Priority pollutants in urban stormwater: Part 1 – case of separate storm sewers. Water Res. 46(20), 6683–6692 (2012). https://doi.org/10.1016/j.watres.2011.12.012
6. Missouri government: "storm drains and water quality". https://extension.missouri.edu/publications/wm6011. Accessed April 2021
7. Monterey government: "Storm Drain Pollution and You". https://monterey.org/Services/Public-Works/Environmental-Regulations/Stormwater-Program/Storm-Drain-Pollution-and-You. Accessed April 2021
8. Inui, T., et al.: Application of toxicity monitor using nitrifying bacteriabiosensor to sewerage systems. Water Sci. Technol. 45(4-5), 271–278 (2002). https://doi.org/10.2166/wst.2002.0603
9. EPSAR: Vertidos industrial. In: Memoria de Gestión 2020, pp. 61–62. EPSAR (2021)
10. Toronto water general manager: "sewers and water supply by-laws 2019 compliance and enforcement annual report". https://www.toronto.ca/legdocs/mmis/2020/ie/bgrd/backgroundfile-156334.pdf. Accessed September 2021
11. Sercu, B., et al.: Sewage exfiltration as a source of storm drain contamination during dry weather in urban watersheds. Environ. Sci. Technol. 45(17), 7151–7157 (2011). https://doi.org/10.1021/es200981k
12. Xu, Z., et al.: Diagnosis of pipe illicit connections and damaged points in urban stormwater system using an inversed optimisation model. J. Clean. Prod. 292, 126011 (2021). https://doi.org/10.1016/j.jclepro.2021.126011
13. Boubiche, D.E., et al.: Advanced industrial wireless sensor networks and intelligent IoT. IEEE Commun. Mag. 56(2), 14–15 (2018). https://doi.org/10.1109/mcom.2018.8291108
14. Gaddam, A., et al.: Detecting sensor faults, anomalies and outliers in the internet of things: a survey on the challenges and solutions. Electronics 9(3), 511 (2020). https://doi.org/10.3390/electronics9030511
15. A survey on anomalies detection techniques and measurement methods. In: 2018 IEEE Conference on Application, Information and Network Security (AINS)' IEEE Conference on Application, Information and Network Security (AINS), pp. 81–86. IEEE (2019)
16. Thiyagarajan, K., et al.: Sensor failure detection and faulty data accommodation approach for instrumented wastewater infrastructures. IEEE Access 6, 56562–56574 (2018). https://doi.org/10.1109/access.2018.2872506
17. Nienhuis, J., et al.: Assessment of detection limits of fiber-optic distributed temperature sensing for detection of illicit connections. Water Sci. Technol. 67(12), 2712–2718 (2013). https://doi.org/10.2166/wst.2013.176
18. Vosse, M., et al.: Processing of DTS monitoring results: automated detection of illicit connections. Water Pract. Technol. 8(3-4), 375–381 (2013). https://doi.org/10.2166/wpt.2013.037
19. Irvine, K., et al.: Illicit discharge detection and elimination: low cost options for source identification and trackdown in stormwater systems. Urban Water J. 8(6), 379–395 (2011). https://doi.org/10.1080/1573062x.2011.630095
20. Li, T., et al.: A reliable sewage quality abnormal event monitoring system. Water Res. 121, 248–257 (2017). https://doi.org/10.1016/j.watres.2017.05.040
21. Baird, R.B., Eaton, A.D., Rice, E.W.: Part 2000 Physical & aggregate properties. In: Baird, R.B., Eaton, A. D., Rice, E.W. (eds.) Standard Methods for the Examination of Water and Wastewater. American Public Health Association, American Water Works Association, & Water Environment Federation (2017)
22. Carminati, M., Luzzatto-Fegiz, P.: Conduino: affordable and high-resolution multichannel water conductivity sensor using micro USB connectors. Sensor. Actuator. B Chem. 251, 1034–1041 (2017). https://doi.org/10.1016/j.snb.2017.05.184

23. Huang, Z., et al.: Design of capacitively coupled contactless conductivity detection sensor. Flow Meas. Instrum. 27, 67–70 (2012). https://doi.org/10.1016/j.flowmeasinst.2012.04.003
24. Kandur, Y., Harms, J., Kern, T.A.: Uncertainty analysis for low-cost transformer-type inductive conductivity sensors. Engineering Proceedings 6(1), 52 (2021)
25. Kang Hui, S., et al.: A new design of inductive conductivity sensor for measuring electrolyte concentration in industrial field. Sensor Actuator Phys. 301(1), 111761 (2020). https://doi.org/10.1016/j.sna.2019.111761
26. Bigham Stephens, D.L., et al.: Regional distribution of Secchi disk transparency in waters of the United States. Lake Reservoir Manag. 31(1), 55–63 (2015). https://doi.org/10.1080/10402381.2014.1001539
27. Prerana, et al.: Design, analysis, and realisation of a turbidity sensor based on collection of scattered light by a fiber-optic probe. IEEE Sensor. J. 12(1), 44–50 (2012). https://doi.org/10.1109/jsen.2011.2128306
28. Yeoh, S., et al.: Plastic fiber evanescent sensor in measurement of turbidity. Sensor Actuator Phys. 285, 1–7 (2019). https://doi.org/10.1016/j.sna.2018.10.042
29. Wang, Y., et al.: Low-cost turbidity sensor for low-power wireless monitoring of fresh-water courses. IEEE Sensor. J. 18(11), 4689–4696 (2018). https://doi.org/10.1109/jsen.2018.2826778
30. Fingas, M., Brown, C.: A review of oil spill remote sensing. Sensors 18(2), 91 (2017). https://doi.org/10.3390/s18010091
31. Arslan, N.: Assessment of oil spills using Sentinel 1 C-band SAR and Landsat 8 multispectral sensors. Environ. Monit. Assess. 190(11), 637 (2018). https://doi.org/10.1007/s10661-018-7017-4
32. Srivastava, H., Singh, T.P.: Assessment and development of algorithms to detection of oil spills using MODIS data. Journal of the Indian Society of Remote Sensing 38(1), 161–167 (2010). https://doi.org/10.1007/s12524-010-0007-9
33. Hou, Y., et al.: Design and implementation of a coastal-mounted sensor for oil film detection on seawater. Sensors 18(2), 70 (2017). https://doi.org/10.3390/s18010070
34. Oh, S., Lee, M.: Oil spill detection sensor using artificial illumination with blue LEDs. In: "2012 IEEE Sensors" IEEE SENSORS 2012. IEEE (2012)
35. "HC-SR04 datasheet," https://cdn.sparkfun.com/datasheets/Sensors/Proximity/HCSR04.pdf%20March, 2021
36. Rocher, J., et al.: A low-cost sensor for detecting illicit discharge in sewerage. J. Sens. 2021, 1–16 (2021). https://doi.org/10.1155/2021/6650157
37. Parra, L., et al.: Development of a conductivity sensor for monitoring groundwater resources to optimise water management in Smart city environments. Sensors 15(9), 20990–21015 (2015). https://doi.org/10.3390/s150920990
38. Basterrechea, D.A., et al.: Low-cost system based on optical sensor to monitor discharge of industrial oil in irrigation ditches. Sensors 21(16), 5449 (2021). https://doi.org/10.3390/s21165449
39. Tektronix: Arbitrary/Function Generator AFG1000 Series Datasheet. https://www.farnell.com/datasheets/2239457.pdf. Accessed January 2022
40. Tektronix: Digital Storage Oscilloscopes TBS1000 Series Datasheet. https://www.farnell.com/datasheets/2053056.pdf. Accessed January 2022
41. Tenma: Digital Multimeter Specifications. http://www.farnell.com/datasheets/1993717.pdf?_ga=2.177994341.1755120939.1591014303-1928794037.1591014303 accessed January 2022
42. Environmental Protection Agency (EPA): Storm Water Management Model (SWMM). US EPA. https://www.epa.gov/water-research/storm-water-management-model-swmm. Accessed January 2022
43. Statgraphics: STATGRAPHICS | Data Analysis Solutions. https://www.statgraphics.com/. Accessed January 2022

How to cite this article: Rocher, J., et al.: Use of wireless sensor network system based on water level, rain, conductivity, oil and turbidity sensors to monitor the storm sewerage. IET Wirel. Sens. Syst. 12(3-4), 103–121 (2022). https://doi.org/10.1049/wss2.12040